Control of wind buffeting vibrations in a suspension bridge by TMD: Hybridization and robustness issues

M. Domaneschi *, L. Martinelli, E. Po

Department of Civil and Environmental Engineering, Politecnico di Milano, Milan, Italy

Accepted 24 February 2015
Available online 11 April 2015

1. Introduction

The modern design of complex structures must be in line with the definition and evaluation of performance, while safety must be assessed under different conditions. Suspension bridges are usually employed for overcoming large distances, requiring to show limited responses against external loads, even if of high intensity. Structural control solutions can contribute effectively to satisfy such levels of performance.

Passive and hysteretic dampers, connecting flexible decks to the supports, represent a feasible solution [8,10–12,14,16]; alternatives are e.g. tuned mass dampers (TMD) or tuned liquid dampers (TLD) along the main girder or at the towers [4,21–23,25,31].

Cyclic buffeting from interaction with the wind is regarded for flexible suspension bridges as a significant excitation due to the low frequencies characterizing both the input and the structure. This paper is based upon a finite element (FE) model of an existent suspension bridge with steel deck, considered in [14] as a case study for performing numerical simulations under strong buffeting wind loading. Wind loading is the main dynamic excitation and is applied on the towers, the cables and the deck, accounting also for motion induced wind forces on the main girder [13]. The wind intensity is tuned at a "storm" level and the multipurpose ANSYS FE code is used as work frame [1].

Following up the research in [17], passive, semi-active and hybrid control strategies are implemented on the suspension bridge FE model for mitigating the wind dynamic effects. A TMD system is studied by means of a simplified two degrees of freedom model for evaluating the optimal configuration and is subsequently applied on the FE bridge model at the deck mid-span for acting on the first lateral mode shape. This first step has been developed accounting for the existent literature on TMD systems

* Corresponding author.

design [6,20,21,25,27,31]. Afterwards, hysteretic dampers are implemented on the suspension bridge between the piers and the deck with passive and semi-active characteristics. These control approaches have completion with the adoption at the same time of TMDs and hysteretic dampers, assembled into a hybrid control scheme with the prospect of ensuring the positive outcomes from both the typologies.

With respect to the original investigation by Domaneschi et al. in [17], the current paper broadens its scope including additional research on the issue of great importance of robustness of control strategies, assessing the proposed control solutions with respect to changes of some of the underlying parameters.

Robustness is herein investigated by evaluating the dynamic response of the suspension bridge model in the case of an out-of-order state of some control devices. Furthermore, the overall performance of the control system is herein first summarized in a robustness index.

2. Structural geometry and numerical model

The suspension bridge model is freely inspired by the Shimotsui–Seto Bridge, in Japan, spanning from the side of Mt. Washu to the Hitsuishijima Island. Fig. 1a shows the main dimensions of the bridge with some details of bridge elements, and connections. Particularly, Fig. 1b shows the bumpers active between the deck and the towers to limit the lateral deck displacement, while Fig. 1c the way the deck is suspended to the towers through a suspension bar at each side of the deck. This bar (vertical black line in Fig. 1c) acts as pendulum in the deck longitudinal direction, allowing for thermal movements, and restrains the deck in the lateral direction though bending. Fig. 2 depicts a general overview of the towers cross-section (Fig. 2a) and the deck end-links at the shores (Fig. 2b).

A view of the FE model adopted for the non linear transient analyses presented in this paper is shown in Fig. 3. This has been developed in the ANSYS FE code. The main simplification herein considered in order to reduce the computational effort of the buffeting analyses pertains to the modeling of the deck, where the real 3D truss structure is replaced by the equivalent "fish-bone" model in Fig. 3. A stiffness based procedure allows to model the original main girder with beam elements of equivalent mechanical properties as the 3D truss.

Timoshenko beam elements, to account for shear deformation, are chosen for modeling the girder and the towers legs (Beam 188 and Beam 44 in the ANSYS element library respectively). The towers are 146 m in height.

Beam elements modeling the main girder are located at the main girder centroidal position and have the following properties:

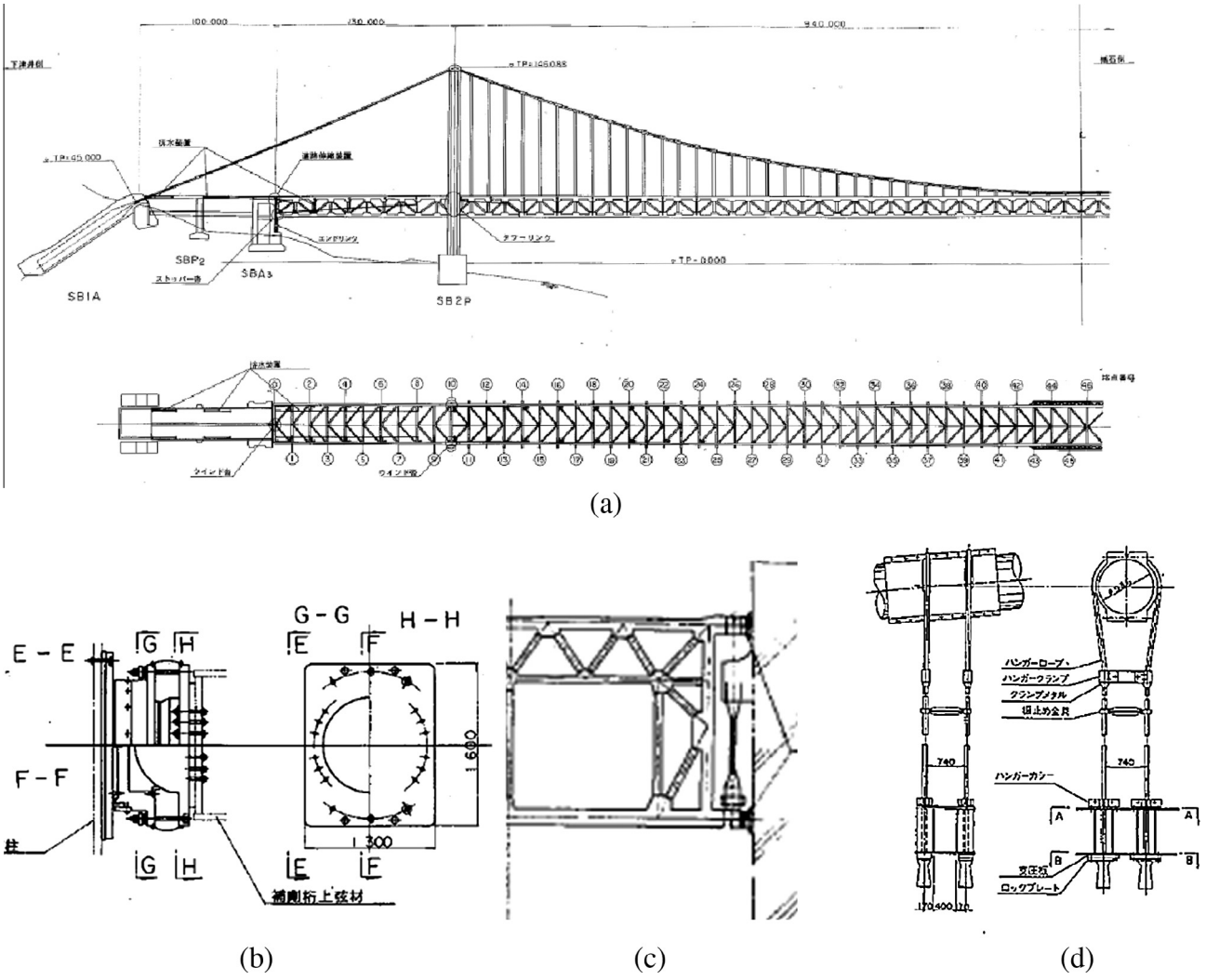

Fig. 1. Bridge geometry (a), flexible bumper between the deck and the towers (b), transversal section of the deck-tower connection (c), suspender-main-cable connection (d). Courtesy of Mr. M. Nishitani HBSE-JP.

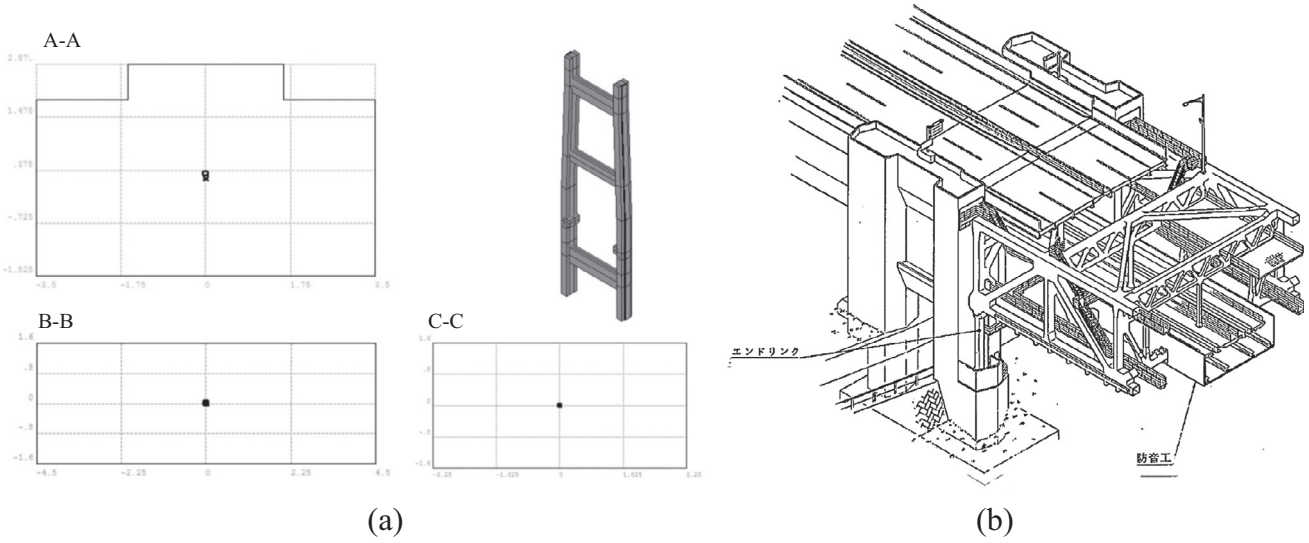

Fig. 2. (a) Cross section of the towers, Section A-A is for the towers' legs (bounding rectangle 7 m × 4.4 m), section B-B (bounding rectangle 9 m × 3.2 m) if for the coupling beam at height 23 m and section C-C (bounding rectangle 6.5 m × 3.2 m) for the coupling beam at height 84 m. (b) General overview of the deck bridge end-links (Courtesy of Mr. M. Nishitani HBSE-JP).

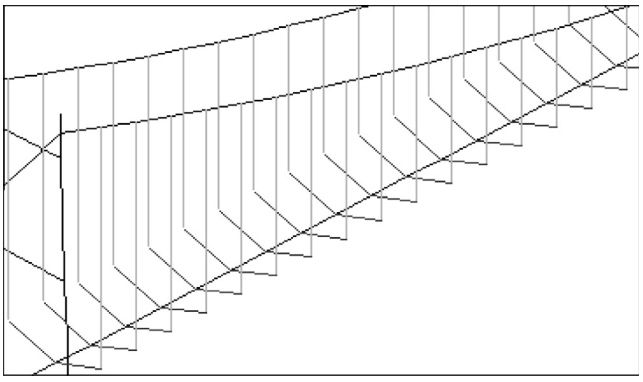

Fig. 3. General view of the "fish-bone" numerical model of the bridge developed for the transient analyses under wind loading.

$A = 0.679\ m^2$, $A_{vx} = 0.195\ m^2$, $A_{vy} = 0.140\ m^2$, $J_x = 16.707\ m^4$, $J_y = 137.141\ m^4$, $W = 348\ kN/m^3$ (resulting in a mass per unit length of the deck equal to 24.08 t/m). The hangers are connected to the main girder elements by rigid elements 18.5 m long, at a spacing of 13 m in the longitudinal directions of the bridge. Hangers and main cables are simulated by tension-only element (element type Link10) [1]. Although the suspenders are two at each suspension point (see Fig. 1d) in the model they are introduced through a single element of diameter 0.17 m. The steel material in the numerical model is different for the cables, the girder and the hangers. For the first two the following values are used: $E = 210{,}000{,}000\ kN/m^2$, $\nu = 0.3$, $\gamma = 78\ kN\ m^{-3}\ g^{-1}$. For the hangers, the values $E = 165{,}000{,}000\ kN/m^2$, $\nu = 0.3$, $\gamma = 70\ kN\ m^{-3}\ g^{-1}$ are adopted, instead. The towers' concrete is characterized by $\nu = 0.2$ and $E = 50{,}000{,}000\ kN/m^2$.

The model is fully restrained to the ground at the towers' foundations and at the ends of the main cables. At the bents, dynamic translations and twist rotation are restrained while the remaining flexural rotations of the main girder are free. The effect of the bumpers in Fig. 1b, employed in the real structure between the deck and the supports for acting on relative displacements, has been neglected in the structural model while the vertical beam of Fig. 1c has been implemented at the deck-tower connection with its original design characteristics. This is the original configuration of the bridge as stated from the design tables and in the following it will be referred to as "Uncontrolled".

A proportional damping matrix is developed for the bridge, aiming at a 1% damping for the first modes involving considerable displacements of the main girder. The damping ratios for several modes are shown in Fig. 4, and are cautionary for a truss steel bridge, as reported in literature [3,18].

The FE model has been validated with the application of the MAC (Modal Assurance Criterion) method [2] against modal data collected on the real structure. The simplified "fish-bone" model shows a fairly good agreement in terms of modal properties (type of modal shape and period of the mode for the first four modes) with data obtained from ambient vibrations testing of the real structure (courtesy of Mr. M. Nishitani, Honshu–Shikoku Bridge Expressway Company Ltd, JP). The first lateral symmetric and first lateral antisymmetric mode shapes are characterized by frequencies of about 0.1 Hz and 0.26 Hz respectively. The other modal shapes identified on the real structure are the vertical antisymmetric and the vertical symmetric one, having frequencies of about 0.16 and 0.20 Hz [13]. The numerical model has been used to perform numerical analyses in time domain of the bridge under buffeting wind loading. For the sake of brevity the interested reader is pointed to literature references for details on the geometry and the ANSYS numerical model [13,14]).

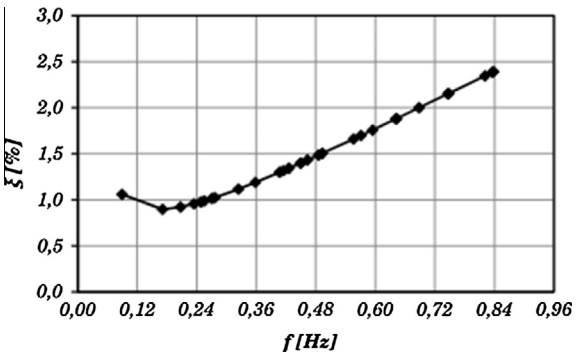

Fig. 4. Damping ratio of the first modes.

3. Wind loading

3.1. Wind field generation

The turbulent component of the wind field is generally function of the orography and the environment. In this work, a three dimensional wind field is used as the base to derive the wind forces on the bridge. The formulation by [24] has been adopted to describe the stochastic turbulent wind field, while realizations are obtained on the base of the wind velocity generation procedure in [7].

The wind field is simulated as a spatially correlated process acting in the horizontal direction, transversal to the deck. According to [24] the Power Spectral Density matrix $\mathbf{S}_V(f)$ of the wind turbulence assumes in this case the shape depicted below, where the n-dimension depends on the number of points in space where wind field has to be evaluated:

$$S_V(f) = \begin{bmatrix} S_{11}(f) & S_{12}(f) & \cdots & S_{1n}(f) \\ S_{21}(f) & \cdots & \cdots & S_{2n}(f) \\ \vdots & \cdots & \vdots & \vdots \\ S_{1n}(f) & \cdots & \cdots & S_{nn}(f) \end{bmatrix} \quad (1)$$

The term S_{ii} on the diagonal represents the power spectral density of the along-wind component of the turbulent velocity, and depends on the average wind velocity v_m, the turbulence intensity $I_u(z)$ in the along wind direction u, on the integral length scale $L_u(z)$, on the height z form the soil (or, in this case the sea surface) of point i [13].

The cross-term S_{ij} represents the cross power spectral density of the same velocity component in the i and j spatial points and comes to depend, besides on $I_u(z)$ and $L_u(z)$, on the distance between points i and j (see [24]).

The integral length scale $L_u(z)$ is a measure of the characteristic dimension of the eddies making up the turbulence, and has the meaning also of the maximum distance of two points after which the turbulence can be assumed as decorrelated.

According to the procedure in [7] the cross power spectral density matrix $\mathbf{S}_V(f)$ of the wind turbulent velocity components is decomposed in its eigenvectors base and a limited number $m < n$ of modal components is retained at each frequency value f_k of interest. The eigenvector matrix $\Psi(f)$ benefits of the following properties: $\Psi^{\mathrm{T}}(f)\,\Psi(f) = \mathbf{I}$ and $\Psi^{\mathrm{T}}(f)\,\mathbf{S}_V(f)\,\Psi(f) = \Lambda(f)$, where the matrix $\Lambda(f)$, of elements $\Lambda_j(f)$, is the diagonal matrix listing the eigenvalues of $\mathbf{S}_V(f)$ at the frequency f.

The contribution of the j-th eigenvector Ψ_j to the turbulent velocity is evaluated as:

$$Y_j(t) = 2\sum_{k=1}^{N} \psi_j(f_k)\sqrt{\Lambda_j(f_k)\Delta f_k}\,[R_k^{(j)}\cos(2\pi f_k t) - I_k^{(j)}\sin(2\pi f_k t)] \quad (2)$$

where $R_k^{(j)}$ and $I_k^{(j)}$ are random variables which have zero mean and variance 1/2 [7]. The real vectors $Y_j(t)$ result n-variate, fully coherent and normal. Then, the complete wind field is approximated at the n points in space through summation of the previous vectors:

$$V(t) = \sum_{j=1}^{m} Y_j(t) \quad (3)$$

A typical time history of wind turbulence obtained in this way is depicted in Fig. 5 where different spectra for the different turbulence components have been used.

3.2. Design mean wind velocity

The value of the average wind velocity for the simulations is taken equal to the design value of wind velocity computed according to the approach in Eurocode 1 [28].

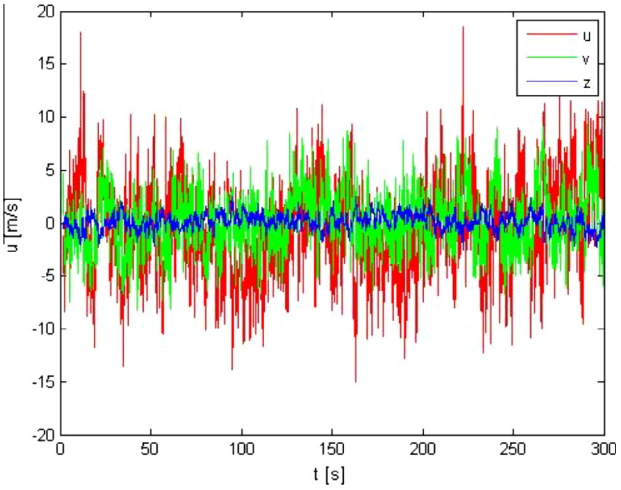

Fig. 5. Sample of realization of the three-component of turbulent wind velocity obtained with the procedure in [7].

One of the main parameters necessary to determine the design wind velocity is the basic value of wind velocity v_b. This takes into account the wind climate for different regions in Europe and corresponds to the characteristic value of 10 min mean wind velocity at 10 m above ground that has an annual probability of exceedance of 0.02 (return period of 50 years). Assuming the orography to be that of a isles and coastal region, a rather high value for the fundamental value of basic wind velocity is $v_{b,0} = 31$ m/s.

The basic value of the velocity has to be transformed into the value at the height of interest on the structure, taking into account the orography. In case of structures located on elevations, like hills, an orography factor $c_o(z) > 1$ takes into account the possible increase in wind velocity.

Velocity at a relevant height, as well as the gustiness of the wind, depends on the terrain roughness. The roughness factor $c_r(z)$ describes the variation of the speed with height z following a logarithmic low:

$$c_r(z) = k_r \ln(z/z_0) \quad (4)$$

To sea or coastal areas (Terrain category 0 in Eurocode 1 [28]) a roughness length $z_0 = 0.003$ m and a terrain factor $k_r = 0.156$ are associated. Consequently, at the height $z = 40$ m of the main girder from sea level the roughness factor becomes $c_r(z) = 1.482$. With a unity estimated orography factor $c_0(z)$, the mean wind velocity is, finally,

$$v_m = c_r c_0 v_b = 1.482 \cdot 1 \cdot 31 = 45.8\ \mathrm{m/s} \quad (5)$$

With the above-assumed coefficients, a 10.5% turbulence intensity I_u and a Lu ≅ 150 m can be calculated.

Similar values were obtained with the approaches in CNR DT207 and WRDSHSB [29,30], see [17] for details.

In light of the small differences stemming from the different procedures, the average wind velocity herein assumed for the numerical simulations on the Shimotsui–Seto Bridge model is 46 m/s. Such value of mean wind velocity is also justified by recordings in the area, characterized by typhoons attack. In the area events with 10 min average wind velocity of more than 45 m/s, and 65 m/s gust velocity, have been registered [19]. Furthermore, the value selected is very close to the one adopted in the bridge design.

It is worth underlining that the wind field adopted in this work represents a new meteorological event with respect previous studies [13,14] from the authors and that the parameters characterizing turbulence are obtained from the selected mean velocity value.

3.3. Wind forces on the bridge

Once the wind field has been completely characterized, the forces due to wind on the structural model can be determined.

In the quasi-static approach drag, lift and aerodynamic torque forces (D_0, L_0, M_0, respectively, see Fig. 6) are generally represented as functions of the relative wind-bridge velocity U and angle of attack α:

$$\begin{cases} D_0 = \frac{1}{2}\rho U^2 B C_D(\alpha) \\ L_0 = \frac{1}{2}\rho U^2 B C_L(\alpha) \\ M_0 = \frac{1}{2}\rho U^2 B^2 C_M(\alpha) \end{cases} \quad (6)$$

In the quasi-static theory, pressure coefficients C (see Eq. (6)) are obtained from static experimental test for different angles of attack. Use of this theory is possible only when aero-elastic effects are negligible. According to the definition of reduced velocity (ratio between wind particle velocity and product between typical deck size, usually the width B, and bridge natural frequency), values greater than 8–10 could allow not to take into account aero-elastic effects. This has been confirmed for this same bridge in [13] where by considering a more refined representation of the wind forces a slight reduction of the bridge response was, nevertheless, obtained. Accordingly, in this work, the drag forces are modeled as a non linear function of the angle of attack while lift and aerodynamic moment are represented by a linear formulation, based on indicial functions, taking into account motion induced wind forces. The use of indicial functions allows expressing, for example, the lift force in a linearized form.

Under the hypothesis of small value changes for the angle of attack ($-5°$,$+5°$), one can consider the McLaurin series expansion of the lift force:

$$L(\alpha) = \frac{1}{2}\rho U^2 B(C_L(0) + C_L'\alpha) \quad (7)$$

Denoting with α_0 the variation of the angle of attack at time $t = 0$, its unexpected alteration will fully induce its effects only after some time. The indicial function $\varphi(s)$ describes this evolution in non dimensional time $s = 2Ut/B$:

$$L(s) = \frac{1}{2}\rho U^2 B C_L'\alpha_0\varphi(s) \quad (8)$$

Normally, the function $\varphi(s)$ is different for lift force and aerodynamic moment, and is approximated by one or more exponential groups of the type $\varphi_i(s) = a_{1,i} - a_{2,i}e^{(-b_{1,i}\,s)} - a_{3,i}e^{(-b_{2,i}\,s)}$ which each depend on five constants. The coefficients $a_{1,i}$, $a_{2,i}$, $a_{3,i}$, $b_{1,i}$, $b_{2,i}$ are estimated by minimizing the differences in case of a harmonic variation of the angle of attack α, and of the horizontal and vertical position of the deck, between the aerodynamic forces computed in time domain using Eq. (8) and the same forces computed in frequency domain using the so called "flutter derivatives". These are extracted from measurements (normally in a wind tunnel) on a sectional model of the bridge cross-section. Full details on the values assigned to coefficients can be found in [13].

Lift force and the aerodynamic moment from the model previously described are applied to the deck members, while the force of drag is applied to the whole structure according to the quasi-static theory.

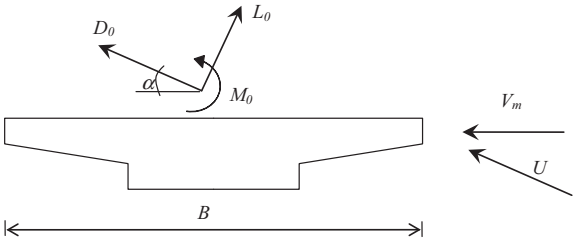

Fig. 6. Quasi-static wind forces on a bridge deck.

The wind forces are applied to the elements' nodes. In particular, the hangers drag force is split in two parts, separately applied to the node common with the main cables and to the one at the deck. The drag component of different elements was calculated according to force coefficient coming from experimental tests (see also [13,14] for details).

4. TMD implementation on the suspension bridge model

4.1. Simplified model: general overview

A TMD is a passive vibration suppression device comprising a mass m, a spring of stiffness k and, frequently, a viscous or hysteretic dampers of damping constant c (Fig. 7a). This type of devices has been widely used in machinery, buildings, and structures [23,25].

The theoretical investigations on the design of TMDs by Den Hartog [6] are probably the most referenced in the literature. Vibrations of a single degree of freedom (SDOF) system may be reduced by introducing an oscillating mass connected to a spring-dashpot device, properly tuned on the dynamical parameters of the main mass (Fig. 7a). For harmonic load acting on the main mass, without any damping, Den Hartog introduced an analytical expression to get the response of a SDOF system equipped with a TMD in terms of amplitude x_1 of the main mass vs. pulsating frequency ω of the external loading excitation. According to Den Hartog the optimal value of the additional mass, which induces the maximum reduction of displacement amplitude, is obtained making the added mass slightly detuned to the main mass.

Ioi and Ikeda [20,22] developed correction factors for the dashpot parameters, as functions of the main mass damping (assuming a light damping of the main mass). In particular, two optimization procedures were proposed: the first one is focused on the reduction of the main mass peak responses, the second one on mitigation of the main mass acceleration. Warburton [27], differently from the others, which focused their approaches on har-monic excitations, investigated the random input loading and sug-gested the TMD's optimum tuning parameters to minimize the response of the main mass.

The presence of viscous damping between main mass and TMD allows a more robust performance when the disturbing frequency is not equal to the resonant one. If the main mass also presents damping, the Den Hartog analytical optimal solutions are not applicable and numerical procedures must be introduced. In this case, more general numerical solutions (frequency domain analysis) for optimal design have been proposed by different authors, as anticipated (e.g. [20–22,25,27]), in terms of tuning parameter f (ratio between TMD frequency ω_a and main mass frequency Ω_n) and damping ratio ξ characterizing the TMD dashpot. These coefficients have been computed for the value of modal mass and period (31,000 t and 11 s) of the first lateral symmetric mode of the bridge, and are plotted versus the parameter μ (mass ratio between TMD mass and main mass) in Fig. 7b and c. In a typical range of mass ratios, normally limited to four percent for practical design purposes, there are no great differences between proposals by different authors, so in the following the values obtained according to the Den Hartog proposal will be used.

4.2. TMD optimal parameters: simplified approach

The same 2DOF simplified system (SDOF with TMD absorber) has been used to investigate the TMD detuning for a TMD positioned at the deck mid-span, acting in transversal direction in

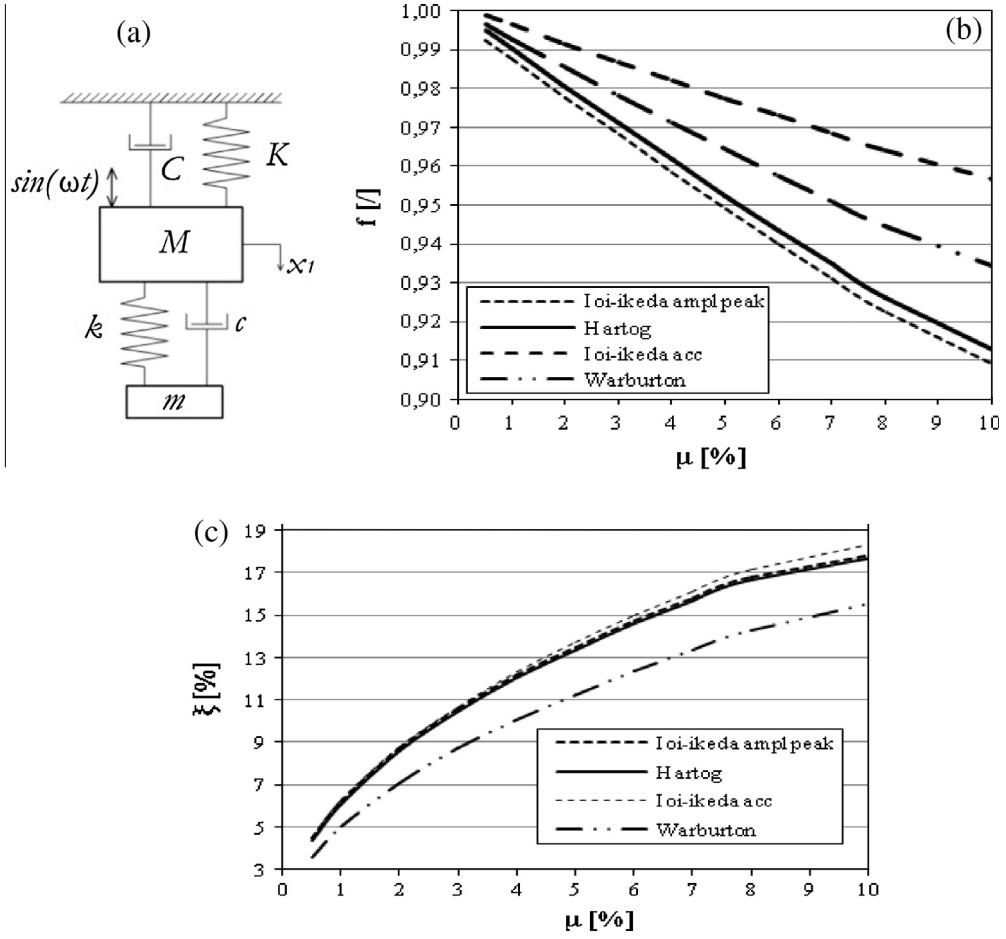

Fig. 7. Solutions for optimal design of TMD device parameters for SDOF system.

the horizontal plane, tuned for controlling the first lateral symmetric mode under wind buffeting loading.

In order to find the optimal TMD parameters some harmonic analyses have been performed on the simplified model of the system. The 2DOF model has been implemented in ANSYS 14 by MASS21 and COMBIN14 elements [1]. The first one represents the TMD mass and the bridge modal main mass. COMBIN14 allows specifying the elastic stiffness and damping parameter. Modal damping of bridge C (Fig. 7a) has been assumed equal to 1% consistently with the damping ratio used in setting up the full bridge damping matrix [18].

Fig. 8 presents the ratio between the maximum displacement amplitude U_t of the controlled main mass and the maximum displacement amplitude U_0 of the mass of the TMD. Applying the Den Hartog tuning equations, the optimal ratio f between the frequencies of the TMD device and of the main mass, and the optimal damping ratio ξ are, respectively:

$$f = \frac{1}{(1+\mu)} \tag{9}$$

$$\xi = \sqrt{\frac{3\mu}{8(1+\mu)}} \tag{10}$$

Fig. 8a shows the behavior of the system, for fixed damping ratios ξ, at the increase of the TMD mass. It underlines that an effective reduction is obtained for damping included in a limited range (lower values). Fig. 8b which presents the ratio U_t/U_0 at the increase of the damping for different masses of the TMD underlines that the optimum damping ξ can be fixed for the TMD mass.

The response at increasing the TMD mass for various values of the tuning parameter f is shown in Fig. 9. Exploring a wide range of values, only coefficients close to unit provide acceptable reduction.

The values of TMD masses reported in Figs. 8 and 9 are limited to less than 10% of mass ratio. This limitation results from a theoretical estimation and also experimental results [21]. When looking at Fig. 9 one can see that the graph for the theoretically achievable reduction has a logarithmic character, meaning the curve flattens with a higher mass ratio so that it becomes less and less effective to increase the mass ratio. Furthermore, in [21] is also shown from experimental results that a higher reduction cannot be achieved by increasing the mass ratio to a value greater than 10%. In light of the relevant masses associated to the first modes of a suspension bridge, for a real bridge application a TMD mass close to 1–2% of the structural one is usually considered [4]. In light of this, in the following transient analyses on the suspension bridge model a mass of the TMD in the range of 1–2% will be considered.

5. Modeling hysteretic dampers

The Bouc–Wen endochronic hysteretic model has often been selected in literature for simulation of dissipative passive and semi-active devices (e.g. metallic dampers, rubber bearings, piezoelectric dampers, magneto-rheological dampers, electro-inductive devices) due to the flexibility of its formulation [8,9,15].

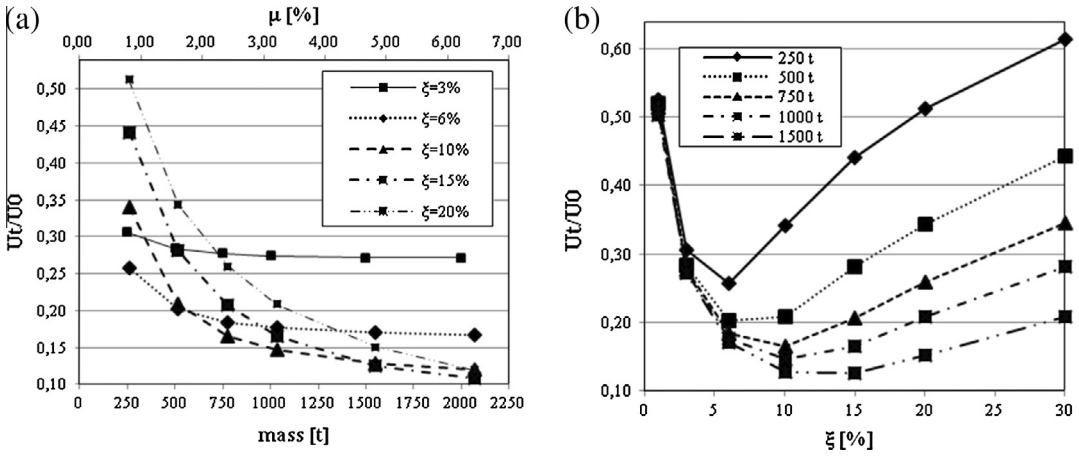

Fig. 8. System behavior for fixed damping ratios ξ (a) and fixed TMD mass (b).

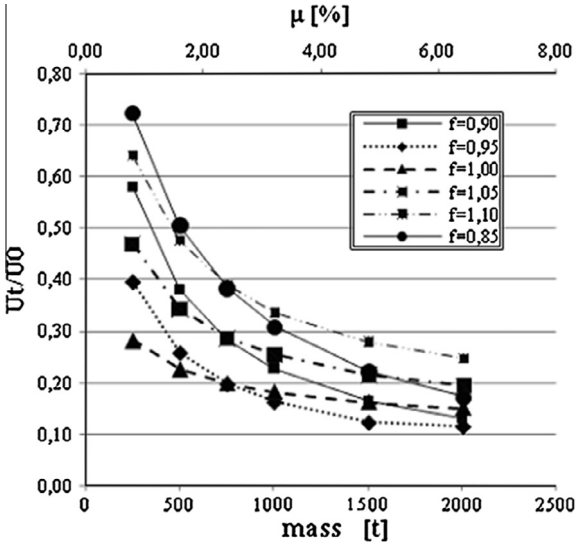

Fig. 9. system response at increasing TMD masses.

According to the original formulation of the model, the equations governing the restoring force produced in each passive device are:

$$\dot{z} = A\dot{x} - \beta\dot{x}|z|^n - \gamma|\dot{x}|z|z|^{n-1} \tag{11}$$

$$\Phi(x,t) = (1-\alpha)kz + \alpha kx + c\dot{x} \tag{12}$$

where x is the relative displacement, z is the auxiliary variable controlling the hysteretic behavior, $\Phi(x,t)$ is the device axial force, $A\ \alpha\ \beta$ n and k are parameters controlling the shape of the cycles and a dot denotes derivation with respect to the time.

The semi-active element is here implemented by using the discrete on/off Skyhook control law. Such algorithm belongs to the class usually employed for controlling semi-active dissipative devices.

Under this condition, the semi-active elements produce control reactions by switching between two force levels. The choice between high or low response level is based on the following control law [8,9]:

$$\dot{x}_{abs} \cdot \dot{x}_{rel} \geqslant 0 \rightarrow \text{high} \tag{13}$$

$$\dot{x}_{abs} \cdot \dot{x}_{rel} < 0 \rightarrow \text{low} \tag{14}$$

Thus, the control forces are defined by two processes: the Bouc–Wen model and the on/off Skyhook control law. The simulated device is semi-active since it is able to change its hysteretic response by increasing or decreasing the elastic limit force. This is obtained acting on the parameters β and γ.

The semi-active on/off SkyHook law can be embedded in the Bouc–Wen formulation through the model proposed in [9]. In the following the semi-active element is formulated with reference to the Shimotsui–Seto Bridge, where x_{tower} and x_{deck} are respectively the absolute displacements of the points at tower and at the deck where the simulated device is connected:

$$\dot{z} = A(\dot{x}_{tower} - \dot{x}_{deck}) - \beta_S H(\dot{x}_{tower} - \dot{x}_{deck})|z|^n - \gamma_{SH}|(\dot{x}_{tower} - \dot{x}_{eck})|z|z|^{n-1} \tag{15}$$

$$\gamma_{SH} = \gamma_{low} - \Delta\gamma H[\dot{x}_{tower}(\dot{x}_{tower} - \dot{x}_{deck})] \tag{16}$$

$$\beta_{SH} = \beta_{low} - \Delta\beta H[\dot{x}_{tower}(\dot{x}_{tower} - \dot{x}_{deck})] \tag{17}$$

$H[\cdot]$ in Eqs. (16) and (17) is the Heaviside step function.

Two values can be assumed by γ_{SH} and β_{SH}, depending whether the high or the low state for damping is required. The increments are defined as $\Delta\gamma = \gamma_{\text{low}} - \gamma_{\text{high}}$ and $\Delta\beta = \beta_{\text{low}} - \beta_{\text{high}}$.

5.1. Optimal passive dampers

The design of passive control dampers for the buffeting low frequency vibrations control of the bridge model is performed through the application of a methodology inspired to the *Sequential Placement Algorithm*. It arises as a prerequisite, the identification of the minimum number of dampers, having as much as possible the same size, so as to achieve the desired structural performance. The identification of the optimal system requires the definition of objective functions and the positioning of control elements. The complete procedure can be found in [14].

The natural and simplest choice for the devices placement is to set them at points where the deck is next to the towers, which are characterized by higher stiffness in comparison to the main girder of the bridge. Those positions are also next to the maximum deck displacements sites.

An interesting parameter on which to act is also the inclination of the dampers with respect to the bridge longitudinal axis. Two classes of dampers are defined, transversal deck dampers, denoted by ST, and longitudinal deck dampers, indicated with SL as shown in Fig. 10. For the last type, two stiffening beams are introduced with the task of creating a support for the insertion of longitudinal dampers at the towers.

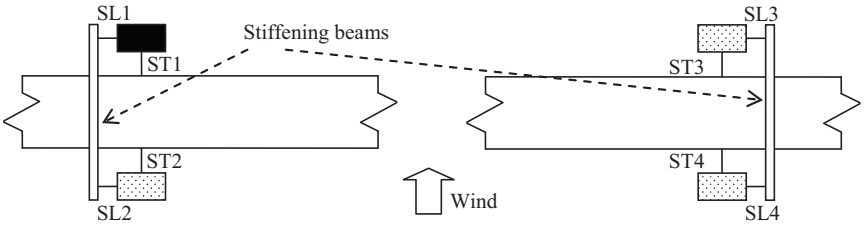

Fig. 10. Devices positioning between deck and towers.

Table 1
optimal parameters for SL and ST devices.

A	n	α	β (m^{-1})	γ (m^{-1})	k (kN m^{-1})	Φ_y (kN)
1	1	0.02	330	330	40,000	60
1	1	0.02	250	250	150,000	300

In [14] it has been shown that the ST devices give the main contribution to the reduction of the predominant transversal deck oscillations while the SL ones play a secondary role by creating a dissipative torque which reduces part of the transverse displacements due to the rotation of the deck around the vertical axis at the towers.

The parameters of the original passive Bouc–Wen model (Eqs. (11) and (12)) representing the control devices are obtained from an optimization procedure carried out considering the design mean wind velocity v_m = 46 m/s. The objective functions are defined as the standard deviation of the internal actions at the base of the towers (shear T_x and bending moment M_z) and the trans-verse mid-deck displacement U_x. Table 1 lists the parameters for the Bouc–Wen model corresponding to the optimal control devices (Φ_y represents the elastic limit force). The complete procedure for the optimal passive control design on the Shimotsui–Seto Bridge model can be found in [14].

In [13] has been show that the optimization procedure performed with a refined wind loading implementation, accounting also for motion induced wind forces, is equivalent in terms of optimal parameters of the control dampers to that obtained with the simplified approach in [14].

5.2. Semi-active decentralized dampers

A semi-active system with hysteretic dampers is studied for the Shimotsui–Seto Bridge with collocated settings adopting the on/off Skyhook control law and the Bouc–Wen model (Eqs. (15)-(17)) [9]. A decentralized scheme, with a low order implementation is adopted, following the theoretical considerations in [8].

Semi-active control devices replace the ST passive ones in the same positions resulting from the optimization presented in the previous section. In this way we tried to ensure, when required, an appropriate enhancement in the damping capacity by increasing the area subtended by the hysteretic cycles.

The ST semi-active devices are characterized at the higher working state by the parameters of the optimal passive case (Table 1). Halved elastic limit, with respect to the optimal one, at the lower working state of the device is considered.

In the collocated setting dampers connect the deck to the piers, which are characterized by high stiffness and therefore subjected to fields of velocity $\dot{X}_{\text{tower}}$ far below those characterizing the deck $\dot{X}_{\text{deck}}$; sensors collect the monitoring data along the same degree of freedom the control forces are applied (Fig. 11).

Additional details on the dampers implementation on the Shimotsui–Seto Bridge can be found in [13,14].

6. Performance evaluation: passive, semi-active and hybrid control strategies

Following the harmonic analyses on the simplified 2DOF model, the efficacy of TMD on the Shimotsui–Seto Bridge model is studied in this section. The bridge is subjected to extreme wind loading characterized by the average wind velocity assumed in Section 3 (46 m/s).

A preliminary assessment on the modal properties of an increase in the bridge total mass due implementing a TMD is reported in Fig. 12 which depicts the lateral frequency and effective mass variation of the Shimotsui–Seto Bridge model adopting different values for the TMD mass. It can be noticed that an increase of the TMD mass involves a decrease in modal frequency. In the range from 250 t to 750 t, the reduction is about 10%. Furthermore, the participating effective mass to the first lateral mode is apparently reduced of about 50% just including a 250 t TMD.

This reduction of modal mass can be simply ascribed to the addition of one degree of freedom to the lateral dynamics of the system.

In order to correctly understand the meaning of the participating mass variation, Table 2 lists the numerical difference in frequency [Hz] with and without the TMD. Preliminarily, it can be observed that higher modes are not influenced by the presence of the TMD. When a single device is added, the second frequency results similar to first one. The mode shape is still similar (lateral, symmetric), while the first vertical mode (which was the second for the w/o TMD configuration) becomes the third in the list. So, the first and second modes result similar in frequency and modal mass also.

In other words, the analysis of changes in modal masses and modal frequencies due to the introduction of TMDs of different masses has pointed out that higher modes are not influenced by the presence of a TMD. When a TMD is added a new mode appears having frequency very close to the first frequency of the bridge without the TMD. The second frequency results similar to the first frequency in the model without the TMD as well. The mode shapes of these two modes remains similar (lateral, symmetric) to that of the first mode in the structure without the TMD while the vertical anti-symmetric mode (which was the second, in the model without TMD) becomes the third in the list. Examination of the modal mass shows that also the cumulated modal mass for the first and second mode remain similar to the mass of the first mode in the structure without the TMD.

The total mass from first and second "damped" lateral modes result very close to the value of the first lateral symmetric undamped mode (~31,000 t).

The implementation of the TMD into the ANSYS FE bridge model (see Fig. 13) consists of two spring-dashpot COMBIN14 elements. These are externally linked with the deck edges and internally to the TMD mass, modeled with a MASS21 element, to allow transversal oscillations of the TMD in the local reference system.

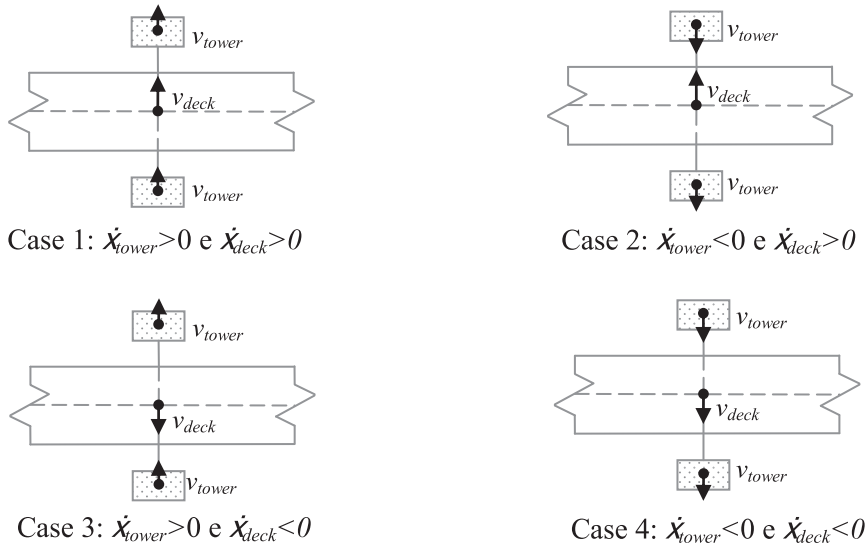

Fig. 11. Skyhook collocated setting.

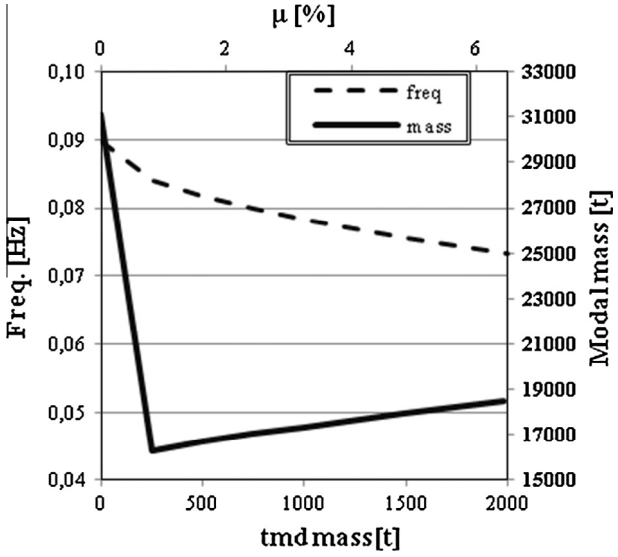

Fig. 12. Bridge natural frequency and effective mass variation vs. TMD mass (b).

Table 2
Frequency natural modes without (w/o) TMD and with different TMD masses.

Mode	w/o TMD (Hz)	TMD 250 t (Hz)	TMD 500 t (Hz)	TMD 750 t (Hz)
1	0.0898	0.0842	0.0818	0.0798
2	0.1716	0.0952	0.0973	0.0985
3	0.2077	0.1722	0.1728	0.1716
4	0.2347	0.2081	0.2085	0.2077
5	0.2483	0.2324	0.2302	0.2347
6	0.2555	0.2502	0.2520	0.2484
7	0.2708	0.2726	0.2743	0.2555
8	0.2766	0.2779	0.2792	0.2710
9	0.3243	0.3237	0.3231	0.2767
10	0.3583	0.3589	0.3594	0.3243

The optimal coefficients inferred by the Den Hartog approach are equally distributed between both COMBIN14 elements.

Considering practicability and encumbrance issues, the TMD mass ranges from 250 t to 750 t. Supposing a concrete mass, characterized by self-weight of 24 kN/m^3, on roller bearing supports like those usually implemented on special structures [25],

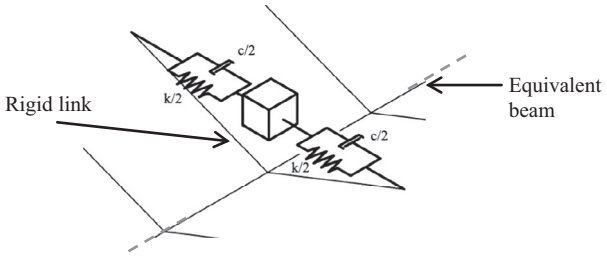

Fig. 13. TMD at the bridge mid-span on the FE model. This model implements an equivalent beam for the main girder.

2 m in thickness and 10 m in width, a maximum longitudinal length for 750 t TMD of about 15 m is required. This total length can be also split in a number of TMD elements, opportunely placed at the mid-span of the suspension bridge.

Different configurations of TMDs have been tested on the FE bridge model, accounting for the preliminary design suggestions coming from the 2DOF system under harmonic excitation (preliminary design). The results are shown in terms of maximum amplitude of mid-span displacements and standard deviation of the same parameter (Fig. 14a and b respectively). They suggest that implementing the specific optimal damping value for the selected TMD mass, gives the maximum response reduction in a time history analysis, even with external loading conditions different from a simple sinusoidal excitation.

Fig. 15 depicts the mid-span lateral displacements of the deck with different configuration of TMDs in terms of mass and corresponding damping ratio.

The bridge dynamics can be controlled not only by a TMD. Passive and semi-active SL and ST dampers may be used alternatively (Section 5). Moreover, hybrid control system, coupling TMD and passive (or semi-active) dampers, are advisable to assure a high level of performance in terms of force and displacement mitigation.

In this light, results in terms of maximum values and standard deviation of mid-span displacement, shear force along the wind loading direction and related bending moment at leeward tower column base are detailed in Tables 3 and 4, giving an overview or the effect of control on the response of the main elements of the bridge.

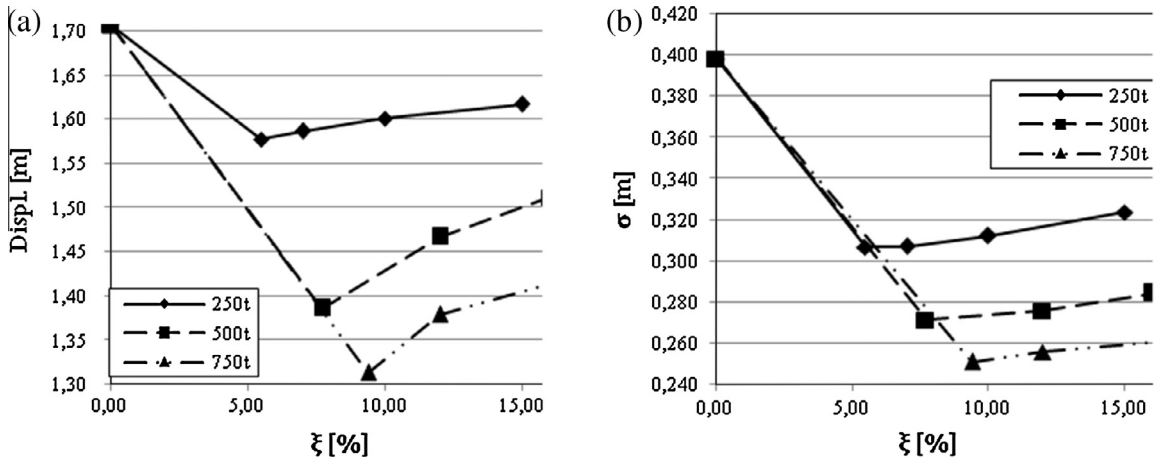

Fig. 14. Maximum amplitude (a) and standard deviation (b) of mid-span displacements as function of TMD mass and damping ratio.

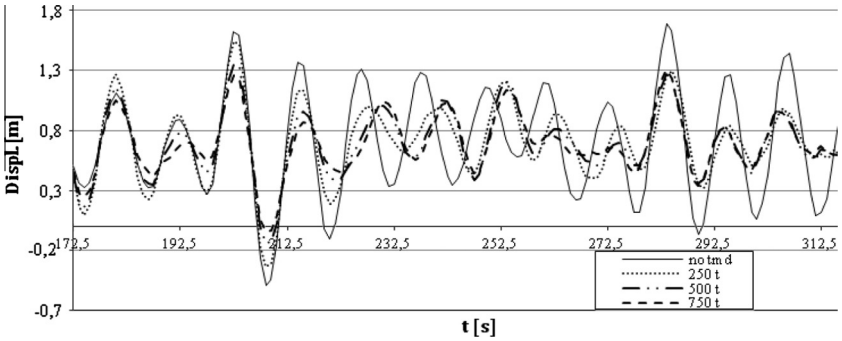

Fig. 15. Mid-span lateral displacements of the deck with different TMDs.

Table 3
TMD or dampers: maximum values and standard deviation of response results in terms of mid-span displacement, shear force along the wind loading direction and related bending moment at leeward tower column base.

Mid-span displ. (m)	NO TMD	TMD OPT	Damper passive	Damper SA low	Damper SA upp
Max					
250 t	1.71	1.58(−7.6)	1.38(−18.8)	1.53(−10.1)	1.28(−24.6)
500 t	1.71	1.38 (−18.8)			
750 t	1.71	1.31(−23.1)			
Standard deviation					
250 t	0.39	0.30(−22.9)	0.26(−33.8)	0.30(−24.3)	0.24(−39.7)
500 t	0.39	0.27(−31.8)			
750 t	0.39	0.25(−36.9)			
Vx node 20,002 (kN)	NO TMD	TMD OPT	Damper passive	Damper SA low	Damper SA upp
Max					
250 t	10,000	9083(−9.2)	9306(−6.9)	9438(−5.6)	9293(−7.1)
500 t	10,000	8991(−10.1)			
750 t	10,000	8783(−12.2)			
Standard deviation					
250 t	1467.8	1243(−15.3)	1211(−17.5)	1279(−12.8)	1183(−19.4)
500 t	1467.8	1167(−20.5)			
750 t	1467.8	1131(−22.9)			
Mz node 20,002 (kN m)	NO TMD	TMD OPT	Damper passive	Damper SA low	Damper SA upp
Max					
250 t	105,640	94,380(−10.7)	96,820(−8.4)	97,720(−7.5)	95,870(−9.3)
500 t	105,640	94,150(−10.9)			
750 t	105,640	91,870(−13.0)			
Standard deviation					
250 t	17,823	15,128(−15.1)	14,682(−17.6)	15,490(−13.1)	14,320(−19.7)
500 t	17,823	14,229(−20.2)			
750 t	17,823	13,804(−22.6)			

Table 4
Hybrid: maximum values and standard deviation of response in terms of mid-span displacement, shear force along the wind loading direction and related bending moment at leeward tower column base.

Mid-span displ. (m)	Hyb. TMD + Passive	Hyb. TMD + SA low	Hyb. TMD + SA UPP
Max			
250 t	1.23(−28.2)	1.29(−24.4)	1.20(−29.3)
500 t	1.21(−29.1)	1.23(−27.8)	1.20(−29.0)
750 t	1.20(−29.6)	1.21(−29.4)	1.21(−29.1)
Standard deviation			
250 t	0.21(−45.4)	0.23(−39.8)	0.20(−48.6)
500 t	0.20(−49.3)	0.21(−45.3)	0.19(−51.7)
750 t	0.19(−51.6)	0.20(−48.4)	0.18(−53.3)
Vx node 20,002 (kN)	Hyb. TMD + passive	Hyb. TMD + SA low	Hyb. TMD + SA UPP
Max			
250 t	9169(−8.3)	9034(−9.7)	9139(−8.6)
500 t	9089(−9.1)	8961(−10.4)	9126(−8.7)
750 t	9031(−9.7)	8920(−10.8)	9069(−9.3)
Standard deviation			
250 t	1099(−25.1)	1129(−23.0)	1088(−25.9)
500 t	1066(−27.4)	1077(−26.6)	1060(−27.8)
750 t	1049(−29.5)	1053(−28.2)	1049(−28.6)
Mz node 20,002 (kN m)	Hyb. TMD + passive	hyb. TMD + SA low	Hyb. TMD + SA UPP
Max			
250 t	95,760(−9.4)	93,800(−11.2)	95,270(−9.8)
500 t	95,100(−10.0)	93,480(−11.5)	95,350(−9.7)
750 t	94,780(−10.3)	93,270(−11.7)	94,770(−10.3)
Standard deviation			
250 t	13,341(−25.2)	13,700(−23.1)	13,179(−26.1)
500 t	12,939(−27.4)	13,076(−26.6)	12,848(−27.9)
750 t	12,746(−28.5)	12,788(−28.3)	12,719(−28.6)

It is worth underlining that the structural responses (displacement and internal forces) have been collected subsequently to the wind loading application, after the initial dynamic transition, when the stationary motion of the bridge is established. Furthermore, at such stationary conditions, the responses are strongly asymmetric due to the asymmetric input loading represented by the wind action, transversal to the deck longitudinal axis. In this light, the maximum value of a variable represents the maximum intensity (maximum absolute value of the response) and it is calculated, as is the standard deviation, in stationary dynamic conditions.

Namely, Table 3 is devoted to TMD systems or dampers implementation, Table 4 to hybrid control systems (percentage reductions in brackets). Mean values are not reported remaining quite equivalent among the different configurations. From Table 3 a similar performance among the exclusive different implementation arises; only the TMD control system with the highest mass seems slightly more efficient than the others.

As detailed in Table 4, hybrid systems allow an interesting performance in terms of response reduction, sometimes revealing themselves as the best performers with respect to the simple TMD configurations or simple dampers implementations. Reductions of about 30% and 50% of the standard deviation of mid-span displacements have been obtained. Benefits arise also in terms of shear forces and bending moments reductions.

Semi-active dampers perform similarly to the passive scheme at the design wind velocity. However, their efficiency comes up at different excitation levels, where they have been proved to be very effective, adapting themselves on line with the loading variation [8,9,14].

Vertical deck displacements at the position of the TMD mass and the relative TMD maximum lateral displacement are also monitored during the transient analyses. An increase of 9% with respect to the vertical deflection at mid-span due to the dead-load is reached with the 750 t TMD. Relative mid-span transversal displacements between optimal-designed TMD mass and the bridge deck give a maximum value of 3.9 m for the 250 t TMD mass. Displacements of 2.50 m and 1.80 m are obtained for the 500 t and 750 t TMD mass, respectively.

In order to achieve a more profound comprehension of the bridge behavior with control devices under wind loading, the power spectral density of the lateral mid-span bending moment has been calculated.

As shown in Fig. 16a, the application of the TMD (to which it corresponds a mass increase of the bridge) does not reduce the frequency content but strongly reduces the amplitudes near the frequency corresponding to the main lateral mode shape. On the other hand, the exclusive presence of dampers (Fig. 16b) makes the bridge stiffener and again reduces the response amplitude. Positive outcomes due to the presence of both TMD and dampers have been detected by the hybrid control system with a 500 t TMD, showing a very interesting reduction in the bridge deck response (Fig. 16c).

An important observation of practical interest, related to the employment of hybrid control systems, can be summarized for the bridge control problem in subject. The adoption of distributed passive and semi-active dampers, between the bridge towers and the deck, in parallel to the TMD, allows to improve the capacity of the structure to preserve desirable levels of performance. Such a control scheme, which belongs to the hybrid typology combining different control devices, may reduce the influence of an out-of-order state for one of them. Under this condition, the reduction in performance due to failure of the Tuned Mass Damper should be more easily counteracted. This aspect, even if typical of the con-trol theory [5], will be demonstrated in detail by the following section.

Finally, it is worth noting that the results herein reported are related to new control implementations against wind loading for

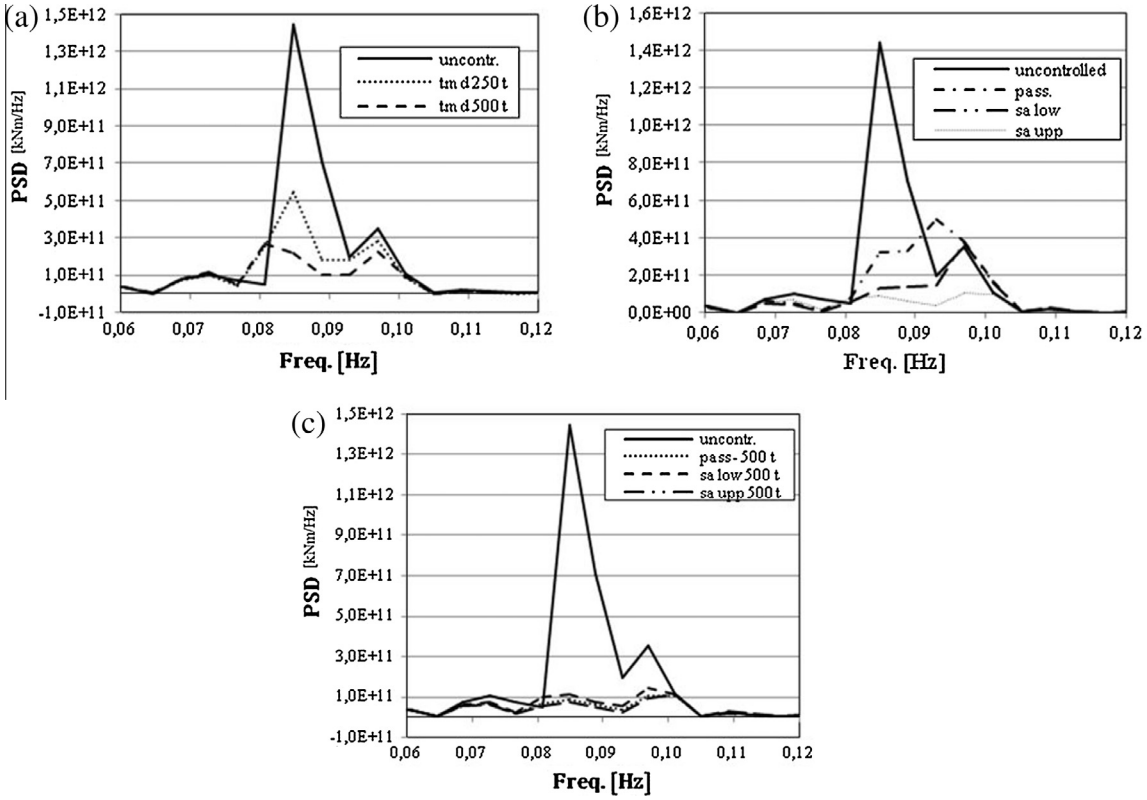

Fig. 16. Power spectral density of lateral mid-span bending moment: TMDs (a), dampers (b), and hybrid (c) control scheme.

large part (TMD solutions and their hybridization). However, when the control system is represented exclusively by hysteretic passive and semi-active dampers, the outcomes corroborate previous observations [13,14]. This is even more interesting considering the wind loading generation, herein developed by the approach in [7], as detailed in Section 3, instead of the different approach implemented in [13,14]. Both numerical solutions, being consistently compared in the hysteretic dampers only configuration, result equivalent.

7. Robustness of the implemented control systems

From a general point of view, robustness can be seen as a specific property of a structure to preserve the same, or a similar, level of performance even if local failures occur [26]. Robustness of con-trol systems on long-span bridges was preliminarily investigated at the numerical level in [8], where the positive outcomes stemming from the devices redundancy and distribution was highlighted. Device redundancy and distribution are also the features exploited in this work to assure presence of the robustness property.

The analyses investigate the deterioration of the response when the TMD is in an out-of-order state, moving jointly with the bridge deck. Variation of the response is tested in two different configurations: first, only with a mid-span TMD; secondly with an hybrid control system in which hysteretic devices at the towers are complemented with a mid-span TMD. In this last option, malfunctioning of the TMD and of the hysteretic dampers are separately modeled.

From a robustness point of view, the control scheme which implements a single device (here the TMD) at mid-span represents the worst arrangement. Failure of the TMD system is simulated as a fixed additional mass on the bridge main girder and it is expected to degrade the performance of the whole system, but being still close to that of the uncontrolled bridge version.

The adoption of distributed passive and semi-active dampers, between the bridge towers and the deck, in parallel to the TMD, it is expected to improve the capacity of the structure to preserve desirable levels of performance. Such control schemes, which belong to the hybrid typology combining different control devices, may reduce the influence of an out-of-order state for one of the devices. Under this condition, the reduction in performance due to failure of the Tuned Mass Damper should be more easily counteracted. Furthermore, hybrid passive control systems have the positive features to assure their passive functioning even if semi-active devices lose their efficacy. This quality is also an interesting feature catching the attention of designers.

Results selected to quantify robustness are presented as absolute values and as variations, mainly with respect to the uncontrolled case (i.e. without any control device). When the hybrid control system is tested, variations with respect to the implementation with only the TMD are also evaluated. Results presented pertain to different response parameters. The lateral dynamics of the bridge deck is monitored by observing the values of displacements in the horizontal plane and the bending moment in the bridge deck in the same plane as well. Base shear forces in the along wind direction, and bending moment about an axis parallel to the deck (i.e. related to the previous shear force) are evaluated for the most stressed tower leg.

Table 5
Simple TMD implementation. Peak responses.

Configuration	Mid-span response		Tower response	
	Displ. (M)	Bending moment (kN m)	Shear force (kN)	Bending moment (kN m)
Uncontrolled	1.52	456,467	8894	92,166
TMD 500 t	1.23	379,431	8044	82,148
TMD 500 t out-of-order	1.54	463,661	8882	91,734

Table 6
Simple TMD implementation. Response standard deviation.

Configuration	Mid-span response		Tower response	
	Displ. (M)	Bending moment (kN m)	Shear force (kN)	Bending moment (kNm)
Uncontrolled	0.34	103,020	1249	15,021
TMD 500 t	0.24	72,826	1058	12,425
TMD 500 t out-of-order	0.35	109,540	1322	15,686

7.1. Schemes with a TMD

Firstly, the damped response caused by presence of the TMD is evaluated. The main response parameters are listed in Tables 5 and 6. The TMD is proven effective also for the base reactions, although the reductions are less important.

It appears that the rigid connection between the TMD and deck (that simulated the TMD out of order state) deteriorates the response in comparison with the situation of a TMD correctly working, since the rigid connection does not allow the relative motion of the TMD mass end hence the correct explication of its control forces. It is worth noting in comparison with the uncontrolled case, which is very similar for masses and boundary conditions, that the response worsens a little.

Fig. 17 compares the time history for mid-span displacements for the uncontrolled case, for the TMD correctly working and for the out-of-order state of the TMD.

By looking at the values in Tables 5 and 6 it can be concluded that, in comparison with the reference case (the uncontrolled one), the TMD on one hand substantially improves the system's response when it is working, while on the other hand it does not excessively deteriorate it when it is in an out-of-order state. It is thus an appealing solution form this point of view.

7.2. Hybrid control scheme

When the TMD is supplemented with longitudinal and transversal hysteretic dampers, an hybrid control system is achieved.

Fig. 18 shows a comparison in terms of displacements of the deck mid-span between the uncontrolled bridge, the bridge with only the TMD control system and different passive, semi-active (ST only, see Section 5) low damping and high damping hybrid solutions. It clearly appears that the last options give a better performance than the tuned mass damper only. Moreover, the best performances are reached with the semi-active control system

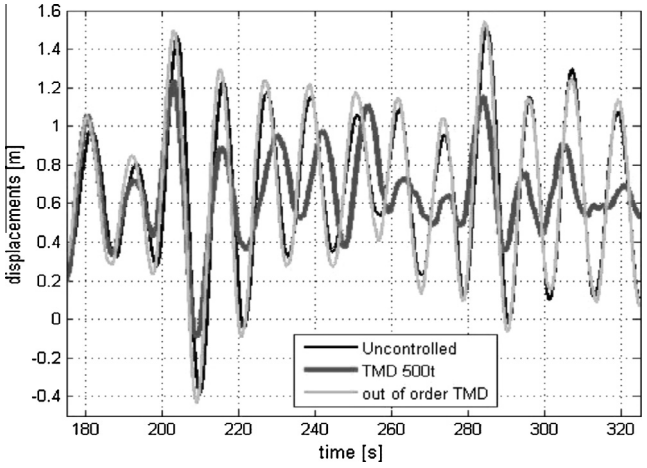

Fig. 17. Time histories of the deck mid-span displacements for the uncontrolled case, the case of a correctly working TMD and the case of a TMD out-of-order state.

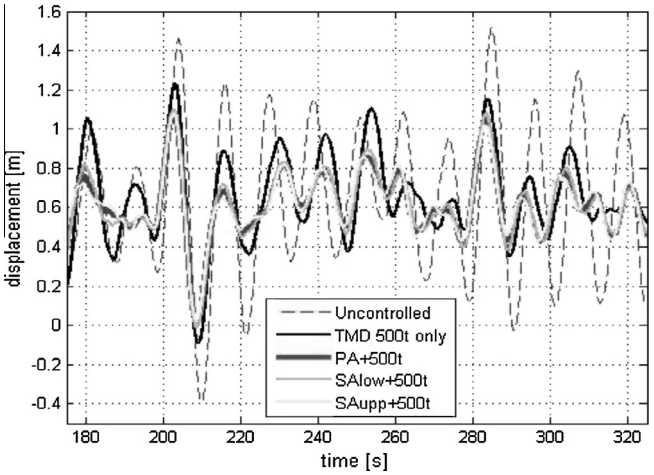

Fig. 18. Time histories of the displacements at deck mid-span for the uncontrolled structural configuration, for the one with only a 500 t TMD active, for the hybrid system TMD – semi-active dampers having low damping capacity ("SA low") and for the one with high damping capacity ("SA upp").

Table 7
Passive dampers + 500 t TMD. Extreme values of response.

Configuration	Mid-span response		Tower response	
	Displ. (m)	Bending moment (kN m)	Shear force (kN)	Bending moment (kN m)
Working hybrid system	1.08	339,160	8224	83,731
TMD o-o-o	1.21	372,900	8314	84,824
ST o-o-o	1.09	337,791	8119	83,440

Note: o-o-o stands for "out-of-order".

Table 8
Passive dampers + 500 t TMD. Standard deviation values of response.

Configuration	Mid-span response		Tower response	
	Displ. (m)	Bending moment (kN m)	Shear force (kN)	Bending moment (kN m)
Working hybrid	0.17	56,430	985	11,451
TMD o-o-o	0.22	71,774	1077	12,601
ST o-o-o	0.19	58,751	959	11,237

Note: o-o-o stands for "out-of-order".

Table 9
Semi-active dampers "SA low" + 500 t TMD. Extreme values of response.

Configuration	Mid-span response		Tower response	
	Displ. (m)	Bending moment (kN m)	Shear force (kN)	Bending moment (kN m)
Working hybrid	1.10	343,870	8089	82,134
TMD o-o-o	1.31	397,640	8247	83,444
ST o-o-o	1.12	341,893	7965	81,156

Note: o-o-o stands for "out-of-order".

characterized by high dissipation capabilities ("SA upp"). This is confirmed by the outcomes listed in Tables 7–12.

In the same tables, the extreme values of the response parameters and the standard deviations of the selected response variables are listed for the case of an out-of-order of the TMD part of a whole hybrid system, together with malfunctioning of one transversal device (either ST passive or semi-active with low or with high dissipation capabilities).

Table 10
Semi-active dampers "SA low" + 500 t TMD. Standard deviation values of response.

Configuration	Mid-span response		Tower response	
	Displ. (m)	Bending moment (kN m)	Shear force (kN)	Bending moment (kN m)
Working hybrid	0.19	59,670	987	11,477
TMD o-o-o	0.24	79,204	1114	13,058
ST o-o-o	0.20	62,173	974	11,401

Note: o-o-o stands for "out-of-order".

Table 11
Semi-active dampers "SA upp" + 500 t TMD. Extreme values of response.

Configuration	Mid-span response		Tower response	
	Displ. (m)	Bending moment (kN m)	Shear force (kN)	Bending moment (kN m)
Working hybrid	1.07	349,730	8163	83,365
TMD o-o-o	1.14	357,060	8278	84,326
ST o-o-o	1.09	345,228	7982	81,611

Note: o-o-o stands for "out-of-order".

Table 12
Semi-active dampers "SA upp" + 500 t TMD. Standard deviation values of response.

Configuration	Mid-span response		Tower response	
	Displ. (m)	Bending moment (kN m)	Shear force (kN)	Bending moment (kN m)
Working hybrid	0.17	55,756	984	11,430
TMD o-o-o	0.20	69,781	1075	12,558
ST o-o-o	0.18	57,648	952	11,154

Note: o-o-o stands for "out-of-order".

Table 13
Robustness Indexes *RI* for the hybrid system with passive devices.

Values used	*RI* type				
	A	B	C	D	E
Max values	1.07	1.05	1.03	1.04	1.03
Standard deviations	1.15	1.16	1.09	1.10	1.10

The TMD malfunctioning implies always a deterioration of the response. On the contrary, the ST damper malfunctioning results of minor significance.

7.3. Robustness index

As a measure of robustness, the results from the previous analysis are recast in terms of a robustness index (*RI*). In principle, it describes the variation of the response, on more than one parameter (i.e. the global base reaction force, or the displacements in different points of the deck), of the out-of-order configuration with respect to the intact structural configuration of the control system. It is evaluated with the extreme values and the standard deviations of the structural variables.

Its analytical expression is defined as:

$$RI = \frac{1}{N_{\text{o-o-o}}} \sum_{i=1}^{N_{\text{o-o-o}}} \sum_{j=1}^{N_{Rp}} \frac{Rp_{j,i}}{Rp_j} \tag{18}$$

Table 14
Robustness Indexes *RI* for the hybrid system with ST "SA low" devices.

Values used	*RI* type				
	A	B	C	D	E
Max values	1.10	1.08	1.05	1.05	1.05
Standard deviations	1.17	1.19	1.12	1.12	1.12

Table 15
Robustness Indexes *RI* for the hybrid system with ST "SA upp" devices.

Values used	*RI* type				
	A	B	C	D	E
Max values	1.03	1.00	1.01	1.01	1.01
Standard deviations	1.14	1.14	1.08	1.09	1.09

where $N_{\text{o-o-o}}$ is the number of out-of-order scenarios envisaged (e.g. malfunctioning of the TMD and intact SL and ST tower-deck dampers, malfunctioning of one ST tower deck damper with intact the other ST ad SL ones and TMD also, etc.), $Rp_{j,i}$ is the j-th response parameter coming form the i-th out-of-order scenario, Rp_j is the same response parameter coming from the structural configuration without malfunctioning, N_{Rp} is the number of response parameters considered in the *RI*. It is worth noting that only one malfunctioning at a time is herein considered.

Different structural variables are considered, combining damper and TMD failures: case A uses the mid-span displacements, while case B uses the lateral mid-span bending moment. Case C combines the mid span displacement and base shear reaction force, while case D substitutes the shear force with the base bending moment reaction. The Last case E is a combination of the all four structural variables. *RI* indexes are listed in Tables 13–15.

The function of the *RI* is mainly at design level for evaluating the best solution in term of robustness among several control systems, coming from preliminary analysis. In this light, from Tables 13–15, the hybrid system with ST "SA upp" devices is the best performer for both extreme responses and standard deviation.

Finally, it is worth underling that when the bridge is equipped with only a TMD the out of order reflect 100% of the control system. Conversely, when the hybrid system is considered, the out-of-order state involve about 10% of the control system (1 device over total 9 ones).

8. Conclusions

Structural control solutions implementing tuned mass damper systems for a suspension bridge are herein detailed through a refined FE model. This is freely inspired to the Shimotsui–Seto Bridge in Japan. A strong wind excitation is simulated as spatial correlated process, acting transversal to the bridge axis in the horizontal plane, accounting also for the steel frame deck motion induced wind forces.

Passive, semi-active and hybrid control schemes are evaluated and their effectiveness is established. The results obtained in part of this study highlight as the presence of a single TMD, positioned at mid-span of the main girder, is able to reduce the bridge response, while not inducing a too large response in case of an out-of-order state of the same TMD. Dampers connecting towers with the deck perform also in satisfactorily way. The hybrid system finally demonstrates itself as the best performer, being able to mitigate both deck displacements and internal forces (lateral bending moment in the steel frame deck, transversal shear with related bending moment at the towers base).

As demonstrated in literature by several research works, the effectiveness of semi-active and hybrid control strategies arises from their capability to adapt to the loading fluctuation allowing better performances when compared to the simple passive ones. Besides, such a type of control solutions guarantees also a residual operational efficiency, as a passive device, if failures occur in the power source.

The use of an hybrid system, encompassing a TMD and passive or semi-active devices, is even more effective in case of a TMD malfunctioning. In fact, there is no response deterioration with respect to the uncontrolled case, but only a reduction in the control system effectiveness. In particular, semi-active devices of high dissipation capacity present the best performances in terms of response reduction and robustness indexes. This trend can also be detected analyzing the values of the robustness index herein firstly proposed for design.

Acknowledgements

Mr. M. Nishitani – Honshu–Shikoku Bridge Expressway Company, Japan – is gratefully acknowledged for making available original data of the Shimotsui–Seto Bridge for the aim of this research work. Dr. C. Meinhardt – GERB Schwingungsisolierungen GmbH & Co. KG, Germany – is also gratefully acknowledged for useful comments on the TMD system.

References

[1] ANSYS. Release 14 user manual. USA: ANSYS Inc.; 2012.
[2] Allemang RJ, Brown DL. A correlation coefficient for modal vector analysis. In: Proceedings of the 1st international modal analysis conference (IMAC); 1982. p. 110–6.
[3] Brownjohn JMW. Estimation of damping in suspension bridges. In: Proceedings of the institution of civil engineers-structures and buildings – Proc Inst Civil Eng-Struct B, vol. 104(4); 1994. p. 401–15.
[4] de Sa Caetano E. Cable vibrations in cable-stayed bridges. Struct Eng Doc (nr. 9), IABSE; 2007, ISBN 978-3-85748-115-4.
[5] Casciati F, Domaneschi M. Semi-active electro-inductive devices: characterization and modelling. J Vib Control 2007;13:815–38.
[6] Den Hartog JP. Mechanical vibrations. New York: Mc Graw Hill; 1956.
[7] Di Paola M, Gullo I. Digital generation of multivariate wind field processes. Probab Eng Mech 2001;16(1):1–10.
[8] Domaneschi M. Feasible control of the ASCE benchmark cable-stayed bridge. Struct Control Health Monit 2010;17(6):675–93.
[9] Domaneschi M. Simulation of controlled hysteresis by the semi-active Bouc–Wen model. Comp Struct 2012;106–107:245–57.
[10] Domaneschi M, Ismail M, Rodellar J, Carusone G, Martinelli L. Characterization, modeling and assessment of Roll-N-Cage isolator using the cable-stayed bridge benchmark. Acta Mech 2013;224:525–47.
[11] Domaneschi M, Martinelli L. Extending the ASCE bridge benchmark: transversal response under seismic loading. J Bridge Eng ASCE 2014;19(3). art. no. 4013003.
[12] Domaneschi M, Martinelli L. Performance comparison of passive control schemes for the numerically improved ASCE cable-stayed bridge model. Earthq Struct 2012;3(2):181–201.
[13] Domaneschi M, Martinelli L. Refined optimal passive control of buffeting induced wind loading of a suspension bridge. Wind Struct, Int J 2014;18:1–20.
[14] Domaneschi M, Martinelli L. Optimal passive and semi-active control of a wind excited suspension bridge. Struct Infrastruct Eng 2013;9(3):242–59.
[15] Domaneschi M, Martinelli L, Perotti F. Wind and earthquake protection of cable-supported bridges, In: Proceedings of the ICE – bridge engineering; 2015, doi: http://dx.doi.org/10.1680/bren.14.00026 [paper 1400026].
[16] Domaneschi M, Martinelli L, Shi C. Aeolic and seismic structural vibrations mitigation on long-span cable-supported bridges. Appl Mech Mater 2013;690–693:1168–71.
[17] Domaneschi M, Martinelli L, Po E. Control of wind induced buffeting vibrations in a long span suspension bridge by TMDs. In: Topping BHV, Iványi P, editors. Proceedings of the fourteenth international conference on civil, structural and environmental engineering computing. Stirlingshire (United Kingdom): Civil-Comp Press; 2013, doi:http://dx.doi.org/10.4203/ccp.102.50 [paper 50].
[18] Gentile C, Martinez y Cabrera F. Dynamic performance of twin curved cable-stayed bridges. Earthq Eng Struct Dynam 2004;33(1):15–34.
[19] Honshu-Shikoku Bridge Authority (HSBA). The Akashi Kaikyo bridge, design and construction of the world's longest bridge. Tokyo, HSBA; 1998.
[20] Ioi T, Ikeda K. On the dynamic vibration damped absorber of the vibration system. Bullet Japan Soc Mech Eng 1978;21(151):64–71.
[21] Meinhardt C. Application of TMD for bridge decks. In: Caetano E, Cunha A, Hoorpah W, Raoul J, editors. Footbridge vibration design. CRC Press; 2009.
[22] Moutinho C. An alternative methodology for designing tuned mass dampers to reduce seismic vibrations in building structures. Earthq Eng Struct Dynam 2012;41:2059–73. http://dx.doi.org/10.1002/eqe.2174.
[23] Nagarajaiah S, Spencer BF. State of the art of structural control. J Struct Eng ASCE 2003;129(7):845–56.
[24] Solari G, Piccardo G. Probabilistic 3-D turbulence modeling for gust buffeting of structures. Probab Eng Mech 2000;16:73–86.
[25] Soong TT, Dargush GF. Passive energy dissipation systems in structural engineering. John Wiley & Sons; 1997.
[26] Starossek U, Haberland M. Approaches to measures of structural robustness. Struct Infrastruct Eng 2011;7(7–8):625–31.
[27] Warburton GB. Optimum absorber parameters for minimizing vibration response. Earthq Eng Struct Dynam 1981;9:251–62.
[28] UNI EN 1991-1-4:2005. Eurocode 1 – actions on structures – part 1–4: General actions – wind actions.
[29] CNR-DT 207/2008. Istruzioni per la valutazione delle azioni e degli effetti del vento sulle costruzioni [in Italian].
[30] WRDSHSB 2001. Wind resistant design standard for HSB.
[31] Ziegler F. Special design of tuned liquid column-gas dampers for the control of spatial structural vibrations. Acta Mech 2008;201:249–67. http://dx.doi.org/10.1007/s00707-008-0062-2.